

Optimization of exposure parameters in full field digital mammography

Mark B. Williams, Priya Raghunathan, Mitali J. More, J. Anthony Seibert, Alexander Kwan, Joseph Y. Lo, Ehsan Samei, Nicole T. Ranger, Laurie L. Fajardo, Allen McGruder, Sandra M. McGruder, Andrew D. A. Maidment, Martin J. Yaffe, Aili Bloomquist, and Gordon E. Mawdsley

Citation: *Medical Physics* **35**, 2414 (2008); doi: 10.1118/1.2912177

View online: <http://dx.doi.org/10.1118/1.2912177>

View Table of Contents: <http://scitation.aip.org/content/aapm/journal/medphys/35/6?ver=pdfcov>

Published by the [American Association of Physicists in Medicine](#)

Articles you may be interested in

[Use of volumetric features for temporal comparison of mass lesions in full field digital mammograms](#)

Med. Phys. **41**, 021902 (2014); 10.1118/1.4860956

[The readout thickness versus the measured thickness for a range of screen film mammography and full-field digital mammography units](#)

Med. Phys. **39**, 263 (2012); 10.1118/1.3663579

[Effects of exposure equalization on image signal-to-noise ratios in digital mammography: A simulation study with an anthropomorphic breast phantom](#)

Med. Phys. **38**, 6489 (2011); 10.1118/1.3659709

[X-ray spectrum optimization of full-field digital mammography: Simulation and phantom study](#)

Med. Phys. **33**, 4337 (2006); 10.1118/1.2351951

[Automatic exposure control for a slot scanning full field digital mammography system](#)

Med. Phys. **32**, 2763 (2005); 10.1118/1.1999107

Educational Lectures

Don't miss these fascinating in-booth speakers. Lectures will be held throughout the show during exhibit hours only, in booth #4001.

Joe Ting, PhD

Utilizing EPID for stereotactic cone commissioning and verification in RIT

Sam Hancock, PhD

Isocenter optimization tools for LINAC-based SRS/SBRT

AAPM 2016 Learn and Earn



Users Meeting

Enjoy some delicious dessert while you learn and earn 2 CAMPEP credit hours at our Users Meeting.

Location . . . Marriott Marquis, Washington, DC

Date Sunday, July 31

Time 7-9 PM

Visit us
at AAPM
Booth #4001



call or visit
719.590.1077 • radimage.com

© 2016, RadImage Imaging Technology, Inc.
2016-07-06

Optimization of exposure parameters in full field digital mammography

Mark B. Williams,^{a)} Priya Raghunathan, and Mitali J. More
University of Virginia, Charlottesville, Virginia 22908

J. Anthony Seibert and Alexander Kwan
University of California-Davis, Sacramento, California 95817

Joseph Y. Lo, Ehsan Samei, and Nicole T. Ranger
Duke University, Durham, North Carolina 27705

Laurie L. Fajardo, Allen McGruder, and Sandra M. McGruder
University of Iowa, Iowa City, Iowa 52242

Andrew D. A. Maidment
University of Pennsylvania, Philadelphia, Pennsylvania 19104

Martin J. Yaffe, Aili Bloomquist, and Gordon E. Mawdsley
Sunnybrook Health Sciences Center, Toronto, Ontario M4N 3M5, Canada

(Received 2 January 2008; revised 31 March 2008; accepted for publication 31 March 2008; published 20 May 2008)

Optimization of exposure parameters (target, filter, and kVp) in digital mammography necessitates maximization of the image signal-to-noise ratio (SNR), while simultaneously minimizing patient dose. The goal of this study is to compare, for each of the major commercially available full field digital mammography (FFDM) systems, the impact of the selection of technique factors on image SNR and radiation dose for a range of breast thickness and tissue types. This phantom study is an update of a previous investigation and includes measurements on recent versions of two of the FFDM systems discussed in that article, as well as on three FFDM systems not available at that time. The five commercial FFDM systems tested, the Senographe 2000D from GE Healthcare, the Mammomat Novation DR from Siemens, the Selenia from Hologic, the Fischer Senoscan, and Fuji's 5000MA used with a Lorad M-IV mammography unit, are located at five different university test sites. Performance was assessed using all available x-ray target and filter combinations and nine different phantom types (three compressed thicknesses and three tissue composition types). Each phantom type was also imaged using the automatic exposure control (AEC) of each system to identify the exposure parameters used under automated image acquisition. The figure of merit (FOM) used to compare technique factors is the ratio of the square of the image SNR to the mean glandular dose. The results show that, for a given target/filter combination, in general FOM is a slowly changing function of kVp, with stronger dependence on the choice of target/filter combination. In all cases the FOM was a decreasing function of kVp at the top of the available range of kVp settings, indicating that higher tube voltages would produce no further performance improvement. For a given phantom type, the exposure parameter set resulting in the highest FOM value was system specific, depending on both the set of available target/filter combinations, and on the receptor type. In most cases, the AECs of the FFDM systems successfully identified exposure parameters resulting in FOM values near the maximum ones, however, there were several examples where AEC performance could be improved. © 2008 American Association of Physicists in Medicine. [DOI: [10.1118/1.2912177](https://doi.org/10.1118/1.2912177)]

Key words: digital mammography, exposure parameters, technique factors, beam optimization

I. INTRODUCTION

The criteria for selection of the optimal target material, external filtration, and tube voltage in full field digital mammography (FFDM) differ from those used in screen-film mammography. This is in part because the separation of the processes of acquisition and display in the former permits the displayed contrast of individual structures to be adjusted when the image is viewed. However, display contrast is limited by the inherent image signal to noise ratio (SNR) because as the displayed contrast of the signal is increased, so is the visibility of noise. Thus, rather than maximization of

contrast within the constraint of acceptable film darkening, which has been the practice in screen-film mammography, beam optimization in digital mammography requires maximization of the image SNR. But since the SNR can be improved almost arbitrarily by increasing the number of detected x-ray photons, exposure parameter optimization must balance increased image SNR with increased patient radiation dose.¹

A critical factor determining both image quality and dose is the spectral composition of the x-ray beam. The energy spectrum is determined primarily by the tube target material,

TABLE I. FFDM units tested. Also listed are the available targets, filters, and the range of kVp values tested along with the corresponding HVLs. kVp is in units of kV and HVL in mm of Al.

Manufacturer	Model	Test site	Target	Filter	kVp range (kV)	HVL range (mm Al)
GE Healthcare	Senographe 2000D	University of Virginia, University of Pennsylvania	Mo, Rh	Mo, Rh	23–39	0.31–0.55
Siemens	Mammomat Novation DR	Duke University	Mo, W	Mo, Rh	23–35	0.2–0.55
Hologic	Selenia	University of Iowa	Mo	Mo, Rh	23–39	0.26–0.44
Fischer	Senoscan	University of Toronto	W	Al	27–42	0.39–0.65
Fuji	5000MA	University of California Davis	Mo	Mo, Rh	24–34	0.27–0.47

the amount and type of internal and external filtration, and the tube's operating voltage (the kVp). Image quality is of course also dependent on the characteristics of the detector, and it is crucial that the x-ray energy spectrum be specifically tailored not only to the physical properties of the breast being imaged, but also to the detector properties (e.g., x-ray absorber thickness and material, scanned versus full area, etc.). For that reason the optimum exposure parameters are likely to be system specific, rather than universal.

In recent years, five manufacturers of FFDM systems have gained FDA approval to market their FFDM system(s), with other manufacturers now in the process of gathering data for application. Most of the approved systems are equipped with automatic exposure control (AEC) mechanisms for automatic selection of at least some technique factors including mA s and in many cases kVp, filtration, and target material. In some units, different acquisition modes are available in which different look-up tables are utilized to emphasize either subject contrast (with lower kVp and higher mA s) or low dose (with higher kVp and lower mA s).

It is the goal of this study to examine, for each of five FDA-approved FFDM systems, the impact of exposure parameter selection on the image SNR and the mean glandular dose (MGD) over a range of breast thickness and composition. The results presented here represent an update of those from an earlier similar study reported at the Fifth International Workshop on Digital Mammography.² At the time of the earlier study, three of the five FFDM systems tested here were unavailable. This article is also a more complete and detailed presentation of results recently reported at the Eighth International Workshop on Digital Mammography.³ Because of the large amount of data, in cases where overall trends were observed that are common to all systems, only representative examples are presented, with more complete system-specific results available in the Appendix, which can be found online through the Electronic Physics Auxiliary Publication Service (EPAPS) of the American Institute of Physics.¹⁶

II. METHODS

II.A. FFDM systems tested

Five commercial FFDM systems located at five different university test sites were used. Table I lists the systems and their test sites, along with the available target, filter, and kVp values for each. The detector of GE Healthcare's Senographe

2000D uses a CsI(Tl) converter coupled to a photodiode thin film transistor (TFT) array. Both the Mammomat Novation DR from Siemens and the Selenia from Hologic use TFT-based detectors overlaid with amorphous selenium. The Fischer Senoscan incorporates a scanned slot-shaped detector based on charge coupled devices fiber optically coupled to a CsI(Tl) converter. Fuji's 5000MA is a storage phosphor (CR) system. For the study described here, the 5000MA was used with a Lorad M-IV mammography unit.

With the exception of the Senoscan, all systems tested had some form of AEC. The AEC on the 2000D (called AOP, or automatic optimization of parameters by GE) can be set up to operate in one of three modes—contrast (*C*), dose (*D*), or standard (*S*) to emphasize contrast, low dose, or both, respectively. In each mode, the target, filter, kVp, and mA s are determined automatically using a brief x-ray pre-exposure. For the Mammomat Novation DR, Siemens recommends the use of the W/Rh target/filter combination for all breast types even though Mo/Mo and Mo/Rh target/filter combinations are also available. Therefore, all AEC testing on the Mammomat Novation DR was performed using W/Rh. The kVp is determined based solely on compressed thickness (with an option for the technologist to override the choice), and the mA s is determined dynamically using a short x-ray pre-exposure. The AEC mode on the Selenia also uses a pre-exposure as well as the compressed thickness of the breast as input to select the filter, kVp, and mA s. The Lorad M-IV used with the Fuji 5000MA was operated in autofilter mode, in which the AEC selects the filter, kVp, and mA s. The mA s selection is affected by a density setting, which was adjusted for CR to get approximately the same entrance exposure to the image receptor as for screen-film (with zero density setting). For this system, the screen-film cassette entrance exposure with a density setting of "0" closely matched the imaging plate entrance exposure with a density setting of "–2," and the latter setting was used for all AEC mode phantom imaging. The requirement for the lower density setting was attributed to the greater attenuation of the Fuji imaging plate and cassette compared to that of screen-film cassettes.

II.B. Phantom design

A common set of phantoms was circulated among the sites, and a common imaging protocol was used. The phantoms were built using a set of blocks of breast equivalent material (CIRS, Inc., Norfolk, VA). The phantom blocks

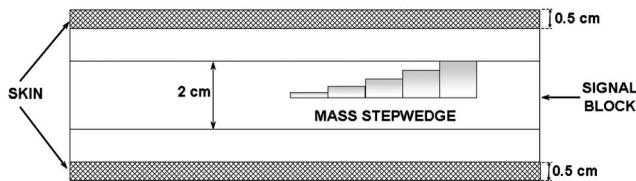


FIG. 1. Schematic side view of a 5 cm phantom with a 2 cm signal block at the center, two 1 cm blank blocks, and two 0.5 cm skins on the surface.

were used to build nine different phantoms, simulating breasts of three different compressed thicknesses (3, 5, and 7 cm) and three different simulated fibroglandular/adipose mass ratios (30/70, 50/50, 70/30). In each assembled stack, the centrally located block (the signal block) contained two step wedges—one each of calcification equivalent material and mass equivalent material. The mass equivalent step wedge had the same x-ray attenuation as 100% glandular material, and the microcalcification step wedge was composed of calcium carbonate. The step wedges were used to simulate breast lesions of different thickness ranging from 0.05 to 0.3 mm thick for calcifications and 2 to 10 mm thick for masses. The thickness of all signal blocks was 2 cm. Above and below the central signal block, blank blocks whose glandular/adipose composition matched that of the background material in the signal block were added to achieve a total thickness 1 cm less than the desired overall phantom thickness. Finally, two 5 mm thick skin blocks, made of 100% adipose equivalent material, were placed on the top and bottom of each stack to simulate skin. Figure 1 is a schematic diagram of a 5 cm assembled stack in cross section. Figure 2 shows a radiographic image of an assembled phantom, illustrating the details of the signal block.

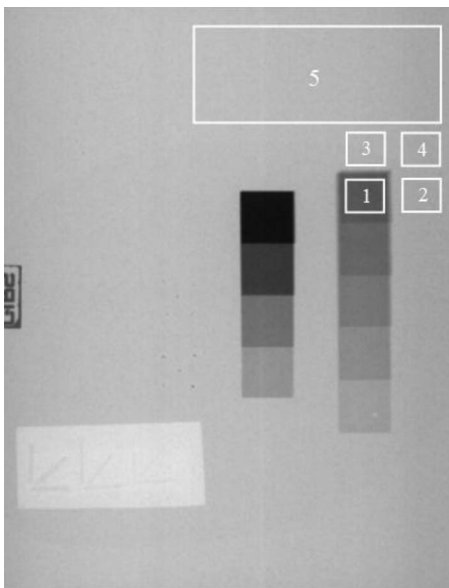


FIG. 2. Image of a phantom showing the calcification (left) and mass equivalent step wedges (the fiber-like objects were not used in this study). The chest wall edge of the phantom is the left edge of the image. The ROIs shown are used for signal and noise calculations (see text).

The chest edge of the image is at the left. The fiber-like objects visible in the image were not used in this study.

II.C. Imaging protocol

The nine phantom types (three compositions \times three thicknesses) were first imaged using the system's AEC. If multiple AEC modes were available, images were obtained using each mode. For FFDM systems in which it was possible to select a specific photocell location (Fuji-Lorad M-IV) or a specific subset of the detector area to be used for AEC purposes (Selenia and Mammomat Novation DR), a region located at approximately the center of the phantom was used.

Following AEC mode image acquisition, images were obtained of each phantom type using either manual mode, in which target, filter, kVp, and mA s were each selected manually, or autotime mode, in which target, filter, and kVp were selected manually, and the AEC system determined the mA s. All target/filter combinations available at each test site were tested. For each target/filter combination tested, an attempt was made to cover the maximum range of kVp's available for that target/filter setting. Exposure times (mA s values) for each phantom/technique combination were selected to give approximately the same average pixel value in the phantom background area as that resulting from AEC mode acquisition. Based on the image data returned, the fluctuations around the average tended to be about $\pm 20\%$ for most sites. The phantoms were positioned at the chest wall edge of the receptor, centered left to right. For each phantom/technique combination, two images were obtained with identical exposure times for the purpose of noise analysis (described below), taking care not to move the phantom between the two exposures.

For the purpose of dose calculation, the half value layer (HVL) thickness and exposure per mA s value (mR/mA s) at a reference point located at a known distance from the focal spot was determined for each target/filter/kVp combination.

II.D. Image analysis

The raw unprocessed DICOM images obtained from each test site were read into a program written in IDL (ITT Visual Solutions, Boulder, CO). The images were cropped leaving only the phantom portion, and equal sized regions of interest (ROIs) were drawn centered on each step. For each step, the signal was defined as the difference between the average analog-to-digital unit (ADU) value in a ROI centered on an individual step (ROI 1 of Fig. 2), and that in an equal sized ROI located immediately adjacent to the step but containing only background (ROI 2). In Fig. 2, ROI 1 is centered on the thickest step of the mass stepwedge. The ROIs of other steps are omitted for clarity. In order to correct for background trends such as the heel effect, two more ROIs of the same size were then defined in the background region (ROIs 3 and 4 of Fig. 2). Their positions were chosen so that they had the same chest-to-anterior locations in the image as ROIs 1 and 2, respectively. The trend-corrected signal was calculated as

$$\text{signal} = [\text{avg}(\text{ROI}_2) - \text{avg}(\text{ROI}_1)] - [\text{avg}(\text{ROI}_4) - \text{avg}(\text{ROI}_3)], \quad (1)$$

where $\text{avg}(\text{ROI}_n)$ denotes averaging the pixel values in ROI number n .

To quantify the image noise, the two images of a given phantom, obtained at a common technique, were subtracted. Image subtraction was performed to remove correlated noise associated with phantom defects, detector nonuniformity, and the heel effect. The root-mean-square (RMS) uncorrelated noise in a single image is then given by the standard deviation of the pixel values in a large background ROI of the difference image (ROI 5 in Fig. 2), divided by the square root of 2,

$$\text{Noise} = \frac{\text{stddev}(\text{ROI}_{5 \text{ diff}})}{\sqrt{2}}. \quad (2)$$

The SNR was defined as the ratio of the signal as defined in Eq. (1) to the noise as defined in Eq. (2).

The MGD for each phantom was calculated using its known thickness, composition and the measured HVL and calculated entrance exposure values for each FFDM system. Entrance exposures were calculated using the mA s value for that exposure along with the measured $\text{mR}/\text{mA s}$ value at the selected reference point, with $1/r^2$ correction to take into account the location of the phantom entrance surface relative to the reference point. For Mo/Mo, Mo/Rh, and Rh/Rh spectra, the parameterized dose tables of Sobol and Wu were utilized to obtain the mean glandular dose per unit entrance exposure, D_{gN} .⁴ For the W/AI spectra, normalized (to entrance exposure) D_{gN} values were obtained from the data of Stanton *et al.*⁵ Their data were extrapolated to 3 cm breast thickness, and interpolation between their published HVL curves was used to obtain correction factors for the particular glandular volume fractions (0.22, 0.40, and 0.61, corresponding to glandular mass fractions of 0.30, 0.50, and 0.70, respectively) used in this study. For the W/Rh spectra, the Monte Carlo calculations of Boone were utilized, interpolating between his published HVL and fibroglandular/adipose composition values.⁶

To study the tradeoff between SNR and exposure or dose, we employ a commonly used figure of merit (FOM) defined as

$$\text{FOM} = \frac{\text{SNR}^2}{\text{MGD}}. \quad (3)$$

The FOM thus defined is independent of the number of photons or exposure (mA s) used to obtain the image in a quantum limited system. Higher values of the FOM indicate the ability of a system to deliver better performance in terms of SNR at a lower dose to the patient, and thus it is useful for deciding among the various acquisition parameter options for a given FFDM system. Thus, this FOM has been used previously by a number of other investigators, in many cases applied to mammographic beam optimization studies.⁷⁻⁹ This FOM is useful for studies such as this one, where the goal is to compare the relative tradeoff between image quality and

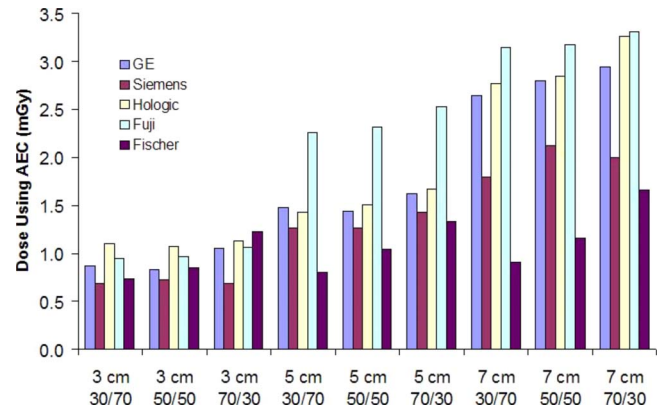


FIG. 3. Mean glandular dose, for each of the breast types studied, delivered by each FFDM system using the AEC mode that automatically selects the greatest number of acquisition parameters. Doses for the Senographe 2000D are those delivered using the Standard AOP mode. For the Senoscan, the doses are those delivered using the manual technique resulting in the highest FOM value for that breast type.

dose for a given imaging system when operational parameters are varied. There are limitations, however, on the value of comparison between imaging systems of the absolute values of the FOM because of system-specific attributes such as the spatial resolution. This and other limitations of this FOM are discussed in Sec. IV C below. In this article all FOM values are reported in units of $(10^{-5} \text{ Gy})^{-1}$ (inverse mrad).

III. RESULTS

III.A. Dose

Although, as might be expected, for a given phantom/target/filter combination, D_{gN} in general increased with increasing kVp,⁶ for all systems the actual MGD was a decreasing function of kVp, since the increasing dose per unit exposure was more than offset by the lower entrance exposures required to achieve comparable average pixel values. Figure 3 shows, for each FFDM system, the dose delivered to a given breast type when the systems are operated using their AECs. Doses shown for the GE system are those when operating in the Standard AOP mode. Since the Fischer system did not have an AEC, the dose delivered using the manual technique resulting in the peak FOM value is shown in Fig. 3.

III.B. Signal

III.B.1. Signal versus step height

In this study the height of the steps in the stepwedges corresponds roughly to lesion thickness. One question is whether the identification of optimum acquisition parameters is dependent upon the lesion thickness, i.e., on the step height. For a given phantom/target/filter/kVp combination, the MGD and noise are independent of step height, so any potential impact on the FOM must come through changes in the value of the signal. Analysis of the images showed, however, that although the magnitude of the signal is clearly dependent on step height, the scaling of the signal with

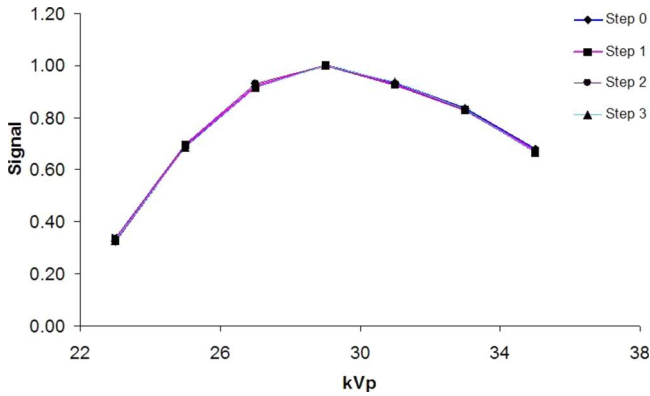


FIG. 4. Normalized signal values for each of the four steps of the microcalcification stepwedge in the 7 cm 50/50 phantom, for the W/Rh target/filter combination of the Novation. The superposition of the four step curves demonstrates that the shape of the FOM curves vs kVp is independent of step height.

changing target, filter, or kVp was essentially independent of step height. For example, Fig. 4 shows, for the Siemens system imaging a 7 cm 50/50 phantom using a W/Rh target/filter combination, the signal plotted versus changing kVp for each of the steps in the calcification stepwedge. Each curve has been normalized by its maximum value to make the kVp dependence easier to compare across step heights. The graph shows that the shape of the curves is virtually identical, suggesting that identification of the optimum kVp is independent of step thickness. In a similar fashion, Fig. 5 illustrates the dependency upon step height of the identification of the optimum target/filter combination. The figure shows, for the example of a 3 cm, 30/70 phantom being imaged by the Senographe 2000D, the signal from each of the steps of the calcification stepwedge, plotted versus kVp for each of the available target/filter combinations. For ease of comparison between target/filter combinations, each signal curve for a given step height has been scaled by a factor

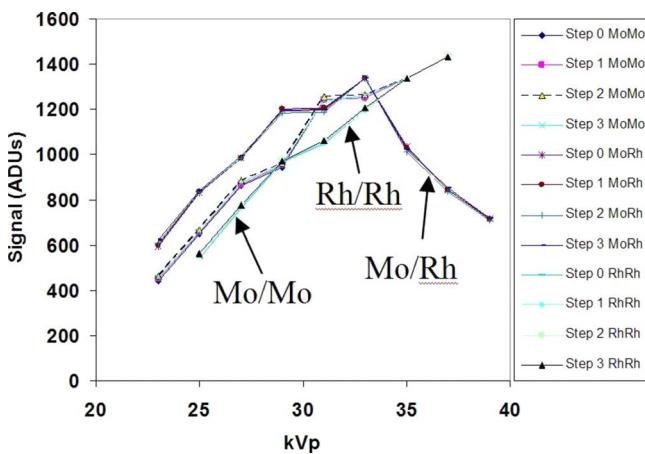


FIG. 5. Normalized signal values for all four steps of the microcalcification stepwedge in the 3 cm 30/70 phantom, for the three target/filter combinations of the Senographe 2000D. The superposition, for a given combination, of the four step curves demonstrates that the measurement of relative target/filter performance is independent of step height.

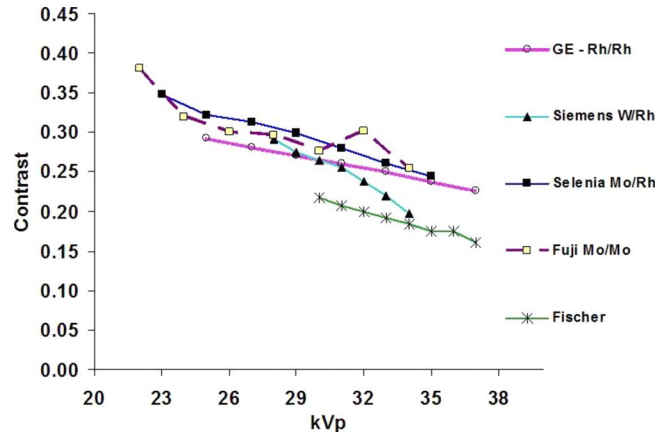


FIG. 6. Contrast vs kVp, 5 cm 50/50, target/filter combinations resulting in the greatest FOM value.

equal to the ratio of the peak signal value in its Rh/Rh curve to that in the Rh/Rh curve of the thickest (0.3 mm) step. Note that the use of the Rh/Rh curves and the signal value of the thickest step for normalization purposes was arbitrary, and similar results are obtained using other target/filter and step choices. The graph shows that determination of the target/filter combination yielding the highest signal (and, hence, the largest FOM) is independent of step height. Given the lack of dependence on step height of the scaling of the signal with changing acquisition parameter selection, for simplicity the results presented in this paper use signal values determined for the 0.3 mm thick microcalcification step only.

As anticipated, subject contrast decreases with increasing kVp due to the decrease in the difference in the linear attenuation coefficients of the step-wedge and background materials. Figure 6 shows, for the target/filter combination of each system resulting in the largest FOM value when imaging a 5 cm, 50/50 breast, the contrast, i.e., the signal normalized by the average pixel value in the background region plotted against kVp. A similar trend (falling contrast with increasing kVp for all FFDM systems) was observed for the other eight breast types tested.

III.C. Noise and SNR

By virtue of the way noise was assessed in this study (via the variance in difference images), only uncorrelated noise contributes to the assessment of the SNR. Uncorrelated noise sources include x-ray quantum noise (primary and scatter), electronic noise, and thermal noise in the detectors. Assessment of the noise alone as a function of changing acquisition parameters is difficult because of the difficulty of controlling the total number of detected x-ray quanta as techniques are changed. Fluctuations in the noise due to changes in the number of detected quanta can be substantially larger than fluctuations due to the impact of the parameter or parameters that have been changed. However, some degree of normalization is possible by assessment of the ratio of the noise to the average background pixel value, or equivalently, assessment of the ratio of the variance to the square of the average pixel value. This type of normalization is similar to that rou-

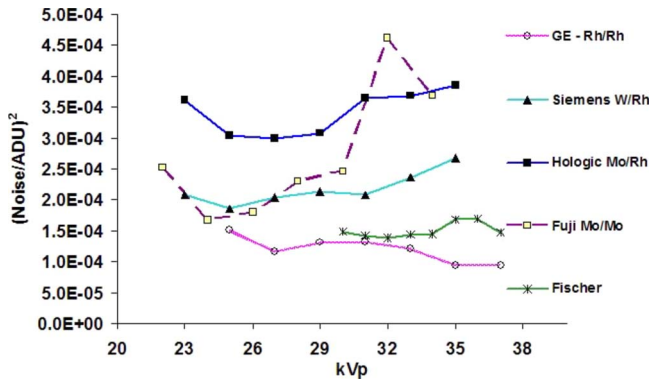


FIG. 7. $(\text{Noise}/\text{ADU})^2$ vs kVp, 5 cm 50/50, target/filter combinations resulting in the greatest FOM value.

tinely performed during noise power spectral analysis, and although it cannot totally eliminate dependency of the measured noise on the somewhat arbitrary mA s selection, it permits the noise in images from acquisition systems with different gains (in ADUs per absorbed x-ray) to be compared. Figure 7 shows, for the case of a 5 cm, 50/50 breast, the square of the noise normalized by the square of the average background pixel value, plotted versus kVp for each FFDM system. These values are numerically equal to the integral of the normalized two-dimensional noise power spectrum. The target/filter combinations resulting in the greatest FOM value for that breast type are shown here. The plots show that the amount of noise varies substantially among the FFDM systems. A similar degree of intersystem variability was observed in the noise when imaging the other eight breast types.

A representative example of the dependence of the SNR on changing kVp is shown in Fig. 8. The graph shows that in general the SNR exhibits a steady decrease with increasing kVp. Similar trends (monotonically decreasing SNR with increasing kVp for all FFDM systems) were observed for the other eight breast types tested with the exception of the thickest (7 cm) breasts. In those cases, the SNR versus kVp curves for the two amorphous selenium FFDM systems (Selenia and Mammomat Novation DR) exhibited peaks around

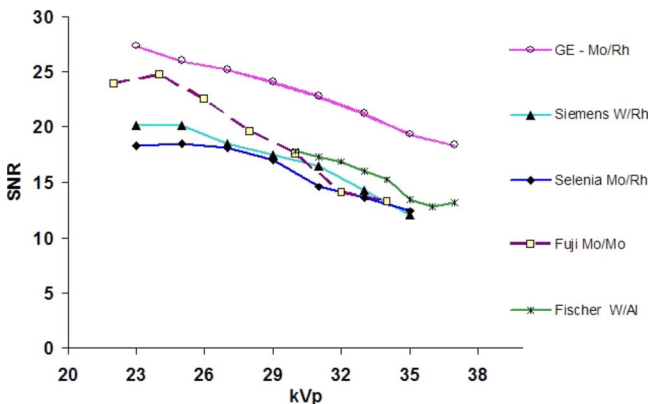


FIG. 8. SNR vs kVp, 5 cm 50/50, target/filter combinations resulting in the greatest FOM value.

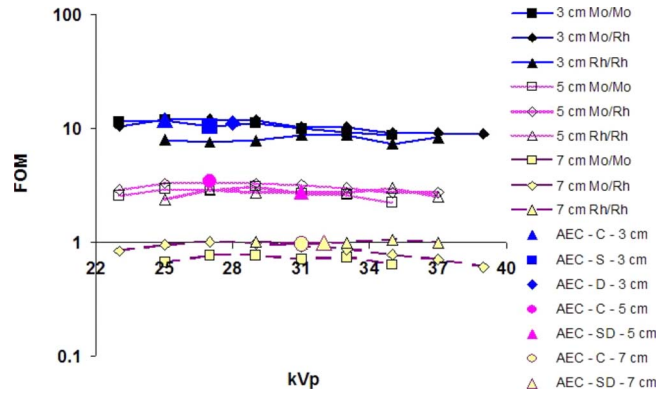


FIG. 9. FOM vs kVp, GE 50/50, all available target/filter combinations.

26–29 kVp, with the SNR steadily falling with decreasing kVp below the peak value as well as with increasing kVp above it.

III.D. Figure of merit

To illustrate the effect of the selection of target, filter, and kVp, on the figure of merit the calculated FOMs for each FFDM system when imaging 50/50 phantoms of all three thicknesses are shown in Figs. 9–13. For all plots except those for the Senoscan, single large symbols indicate the technique chosen by that system’s AEC for each phantom type. Similar FOM plots for the 30/70 and 70/30 composition phantoms, along with reproductions of Figs. 9–13 can be found in the Appendix (Figs. A1–A15). Table II summarizes, for each FFDM system, the technique factors that produced the maximum FOM for each breast type, and the resulting HVL.

IV. DISCUSSION AND CONCLUSIONS

IV.A. Figure of merit

Figures 9–13 for 50/50 breast composition, and Figs. A1–A15 in the Appendix for all three compositions, show that in most cases the FOM is not a strong function of kVp, and that in those cases where the FOM does exhibit a peak as a function of kVp, it is broad. On the other hand, the FOM is much

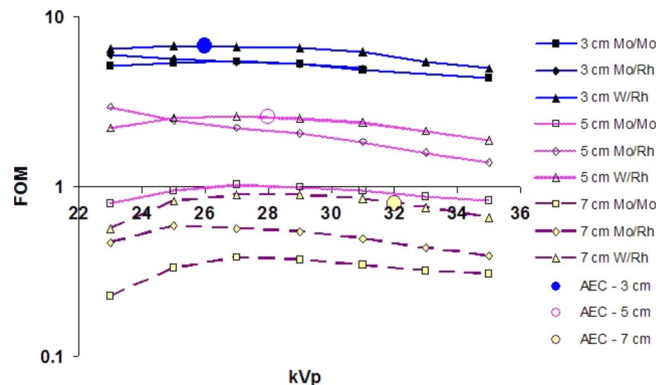


FIG. 10. FOM vs kVp, Siemens 50/50, all available target/filter combinations.

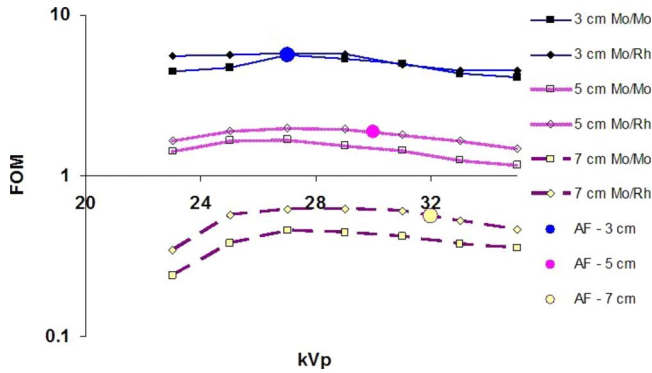


FIG. 11. FOM vs kVp, Hologic 50/50, all available target/filter combinations.

more strongly determined by the choice of the target/filter combination. The fact that in all cases the FOM is a decreasing function of kVp at the upper end of the kVp range tested here suggests that, at least for the target/filter combinations currently included in these FFDM systems, there is no advantage in expanding the available voltage range to even higher kVp.

Comparison of Tables I and II shows that, for a given breast type, the HVL of the technique producing the highest FOM tended to fall at a location within the range of available HVL values that is quite system-specific. For the Senoscan and 5000MA system, the optimum techniques had HVL values that increased with increasing breast thickness but were always in the lower half of their available HVL ranges. On the other hand, for the Mammomat Novation DR, the optimum technique factors were nearly identical for all breast types, always utilized the W/Rh combination, and corresponded to a HVL that was near the top of its available range.

Compared to the Novation DR, the HVLs of the optimum techniques for the Senographe 2000D were more distributed but lay only in the upper half of the available HVL range. Notably, the maximum FOM was always obtained with either Mo/Rh or Rh/Rh target filter combinations but never with Mo/Mo, even for the thinnest and most fatty breasts.

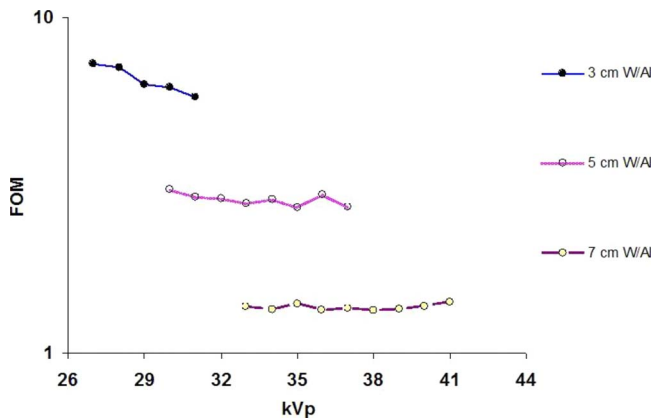


FIG. 12. FOM vs kVp, Fischer 50/50, all available target/filter combinations.

TABLE II. Summary of exposure parameters resulting in the highest FOM value for each FFDM system, for each of the nine breast types tested. Parameters are in the form target/filter/kVp/HVL, with kVp in kV and HVL in mm Al.

	Thickness (cm)	30/70	50/50	70/30
GE	3	Mo/Rh/27/0.43	Mo/Rh/27/0.43	Mo/Rh/27/0.43
	5	Mo/Rh/27/0.43	Mo/Rh/27/0.43	Mo/Rh/27/0.43
	7	Mo/Rh/27/0.43	Rh/Rh/31/0.48	Rh/Rh/33/0.53
Siemens	3	W/Rh/27/0.49	W/Rh/27/0.49	W/Rh/29/0.51
	5	W/Rh/27/0.49	W/Rh/27/0.49	W/Rh/29/0.51
	7	W/Rh/27/0.49	W/Rh/29/0.51	W/Rh/29/0.51
Hologic	3	Mo/Rh/27/0.39	Mo/Rh/27/0.39	Mo/Rh/27/0.39
	5	Mo/Rh/27/0.39	Mo/Rh/27/0.39	Mo/Rh/27/0.39
	7	Mo/Rh/27/0.39	Mo/Rh/28/0.40	Mo/Rh/28/0.40
Fischer	3	W/AI/27/0.42	W/AI/27/0.42	W/AI/27/0.42
	5	W/AI/29/0.45	W/AI/30/0.46	W/AI/30/0.46
	7	W/AI/35/0.54	W/AI/35/0.54	W/AI/35/0.54
Fuji	3	Mo/Mo/24/0.30	Mo/Mo/24/0.30	Mo/Mo/26/0.32
	5	Mo/Mo/24/0.30	Mo/Mo/24/0.30	Mo/Mo/26/0.32
	7	Mo/Rh/28/0.43	Mo/Rh/28/0.43	Mo/Rh/28/0.43

The Selenia produced maximum FOM values for nearly all breast types at an exposure parameter setting of Mo/Rh, 27 kVp, with only a slightly higher kVp (Mo/Rh, 28 kVp) for the two densest 7 cm breasts. As might be expected, the FOM values for the Mo/Mo and Mo/Rh target/filter combinations were very similar to those of the Novation DR using the same target/filter combinations, since the Selenia and Novation DR use the same detector type. However, for all breast types the FOM values obtained by the Novation DR using the W/Rh combination were superior to those using either Mo/Mo or Mo/Rh.

Contrary to the Senographe 2000D and the Selenia, the maximum FOM was obtained for the 5000MA with a Mo/Mo combination for most (6 of 9) breast types, with only the 7 cm phantoms benefiting more from Mo/Rh. However, the performance of these two target/filter combinations was

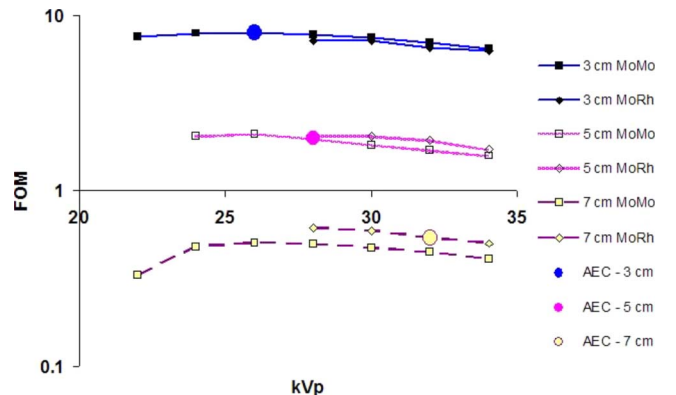


FIG. 13. FOM vs kVp, Fuji 50/50, all available target/filter combinations.

fairly similar for the 5000MA, whereas for the Selenia Mo/Rh provided a distinct advantage over Mo/Mo.

Comparison of plots of the noise (Fig. 7 for the 5 cm 50/50 breast type) and those of the FOM (Figs. 9–13) shows a general inverse correlation between the normalized noise and the FOM, with higher noise systems tending to have lower FOM values for a given breast type. A similar correlation was observed for the other breast types. This correlation suggests that the relative system noise is an important determinant of relative FFDM system performance, irrespective of signal and dose performance. The relatively low noise of the Senographe 2000D in part results in high FOM values, especially for 3 and 5 cm thick breasts.

IV.B. AEC performance

Figure 3 shows that there is a substantial difference among FFDM systems in the radiation dose delivered under AEC operation. In general the combined Fuji-Lorad system delivers the highest dose under AEC operation of all the systems tested, while the Novation DR delivers the least of all systems with AECs. It is important to remember that the dose when using the Fuji system depends on the physical characteristics (antiscatter grids, internal x-ray tube filtration, compression paddle, etc.) of the screen-film unit it is being used with, and also on its AEC look-up tables and the specific operating parameters chosen. For example, in this study a density setting of -2 was chosen so that the imaging plate cassette entrance exposure approximated that of the screen-film cassette used with a density setting of 0; however, other choices are certainly possible. System-to-system variability is minimized to a large degree, however, by adherence to the guidelines for maintaining the expected SNR and CNR as stipulated in the Fuji quality control manual.

The Senoscan, operated with kVp settings close to those maximizing the FOM for that system, delivers the lowest radiation dose of all systems tested for 5 and 7 cm breasts. This dose advantage is a product of the intrinsic scatter rejection of the scanned slot design and the relatively energetic W/Al beam.

Inspection of Figs. 9–13 for 50/50 breast composition (and Figs. A1–A15 for 30/70, 50/50, and 70/30 compositions) indicates that in most cases, the AECs of the FFDM systems identified exposure parameters producing FOM values fairly near to the maximum ones attainable. However, there are several ways in which AEC performance might be improved for some FFDM systems.

For the Selenia, the FOM for the Mo/Rh combination is superior to that for the Mo/Mo combination at virtually any voltage for all breast types. Since the AEC selected Mo/Mo for 3 and 5 cm breasts of all compositions, it also suggests that dose performance could be improved without loss of image quality by programming the AEC for selection of the rhodium filter for smaller breast thickness.

The decision by Siemens to recommend the W/Rh target filter combination during AEC mode acquisition on the Mammomat Novation DR appears well motivated, since that combination outperformed Mo/Mo and Mo/Rh for all breast

types imaged. As noted above, the AEC's preliminary kVp selection is based solely on compressed breast thickness and is thus insensitive to changing breast composition, and the same target/filter/kVp would be chosen for all breast compositions of a given thickness. The FOM curves suggest that compared to the default AEC selections, some performance improvement may be possible through the utilization of somewhat lower kVp settings for thicker (i.e., 7 cm or thicker) breasts with only minimal increase in MGD. This would be readily achievable since the option exists to override the AEC's preliminary kVp selection.

For the Senographe 2000D, the best FOM values for all 3 cm phantoms were obtained with the Mo/Rh target/filter combination. However, the AEC selected Mo/Mo for all 3 cm phantoms in all three modes, resulting in lower FOM values.

In some cases, especially for very thin or very thick breasts, the techniques selected by the AEC system of some FFDM units produced a FOM value that was noticeably lower than that possible using another technique available to that FFDM system. In these cases, it would not be unreasonable for the medical physicist to point out these results to sites with the suggestion that modified techniques be considered for relevant breast types and to work with service personnel to adjust AEC calibration accordingly. For example, Siemens has configured the AEC software of the Mammomat Novation DR so that the selection of the default kVp and target/filter combination as a function of compressed breast thickness can be set up according to the site's preferences. Ideally, the results of optimization studies such as this and other similar studies will serve as input to FFDM manufacturers as they continue to develop the AEC programming in the upcoming years.

It should be remembered that FFDM is still relatively new, and that partially for practical manufacturing reasons most of the target/filter combinations available on the FFDM units tested are the same as those on the contemporary screen-film units of the same manufacturer. It is likely that the target and filtration combinations available for these systems may change in the future as experience is gained with the detectors.

IV.C. Study limitations and sources of uncertainty

Uncertainty in the measured values of the HVL or entrance exposure results directly in uncertainty in the calculated MGD. Fortunately, both of these quantities are smoothly changing functions of kVp, so errors in the measurements were relatively easy to detect, and in several cases remeasurement of the HVLs for all techniques used for phantom imaging was performed.

In most cases the FOM is a smoothly changing function of kVp. However, for the Senographe 2000D fluctuations existed in some of the FOM curves that were nearly equal in magnitude to the separations between the curves corresponding to different target/filter combinations, thus making determination of the acquisition parameters producing the maximum FOM difficult. Noise power spectra from a sequence of

difference images showed two well-defined peaks located symmetrically on the primary axis corresponding to the left-right direction in the images. Such peaks suggest the presence of periodic noise such as stripes running in the chest-anterior direction. However, the magnitude of this periodic noise changed from one difference image to another. One possible explanation is that the noise was due to the antiscatter grid, whose septa run in the chest-anterior direction. This theory was given credence by the fact that the noise power spectrum (NPS) of images obtained with the grid removed did not contain the peaks. The fact that the noise was present in varying degrees in difference images obtained from successive pairs of phantom images suggests that the exact locations in the image of the grid structure might vary between two successive exposures obtained using identical exposure parameters, and therefore cancel to varying degrees during the subtraction process. It should be noted that even in cases where the magnitude of the periodic noise was relatively large, no grid line artifacts were visible in either the individual or difference images, and thus their impact on image quality is not likely to be clinically significant. However, the image-to-image fluctuations in the grid noise were of sufficient magnitude to produce the fluctuations observed in the FOM values.

The phantom construction and image analysis used in this study result in a large-area (low spatial frequency) assessment of signal as the difference of average pixel values in relatively large ROIs centered within the stepwedge steps. Similarly, quantification of noise only by way of the RMS pixel-to-pixel fluctuations precludes analysis of spatial frequency dependence of the noise. These are not limitations for achieving the goals of this study, namely studying the effect of changing exposure parameters on contrast and dose for a given FFDM system. However, it is important to bear in mind, when comparing the FOM values of different systems that the nature of the test determines the numerical range of FOM values within which each system operates. For example, this definition of SNR could result in higher FOM values for systems in which the x-ray quantum noise is smoothed by the system modulation transfer function (MTF), since there is no accompanying penalty for smoothing the signal. A complete frequency-dependent description of system performance could in principle be undertaken through measurement of the MTF and NPS to characterize signal and noise, respectively, and by determination of the number of noise equivalent quanta as a measure of the (square of the) SNR.

In clinical imaging, breast structure noise can be a significant factor determining lesion visibility. It is possible that the nature (spatial frequency composition, x-ray attenuation, and spatial distribution) of the structural noise could have an impact on the identification of optimum acquisition parameters. The phantoms employed in this study had uniform (structureless) background regions, and only uncorrelated noise was assessed in the determination of image SNR. There were several reasons that uniform-background phantoms were used. First, there are no currently available phantoms for digital mammography that model breast structure noise. Sec-

ond, and most importantly, even if such a phantom existed, it would not be appropriate for this study, which has as one of its primary goals evaluation of the AEC performance of the current FFDM systems. Since these systems do not perform a spatial-frequency dependent analysis of factors such as breast structure noise, our results would be heavily biased by the particular phantom structure chosen, and thus it would be very difficult to compare them to AEC performance.

This study did not take into account the exposure times associated with each of the exposure techniques tested. Exposure time could potentially be included in a more elaborate figure of merit since the likelihood of motion artifacts increases with increasing exposure time.

In the clinical setting, many different image processing algorithms are ultimately applied to the raw (for processing) images that were analyzed in this study. These algorithms are manufacturer specific and have a variety of purposes (thickness compensation, contrast enhancement, MTF compensation, logarithmic transformation, etc.). While it is beyond the scope of this study to determine the impact of these various image processing techniques on image quality, they can influence the contrast, effective dynamic range, spatial resolution detail, edge response, presence of artifacts such as halos (e.g., undershoot and overshoot), and noise of the image ultimately viewed by the radiologist. The impact of these factors has been shown to depend on radiologist experience level and viewing preferences.¹⁰⁻¹²

IV.D. Comparison with previous studies

A limited number of beam optimization studies have previously been performed for individual FFDM systems. Lo *et al.* utilized an approach and a FOM similar to those described here to compare the image quality and dose performance for Mo/Mo and W/Rh target/filter combinations on an early prototype of the Mammomat Novation DR.⁹ In agreement with the results presented here, they found that W/Rh consistently outperformed Mo/Mo for 4, 6, and 8 cm breasts of 0%, 50%, and 100% fibroglandular composition. The superiority of this target/filter combination for the Novation DR has recently been confirmed through simulation and phantom experiments by Bernhardt *et al.*¹³ Geertse *et al.* imaged 3, 5, and 7 cm poly(methylmethacrylate) blocks and a CD-MAM phantom on a Selenia.¹⁴ They reported superior contrast-detail performance for all three thicknesses using a Mo/Rh target/filter combination compared to Mo/Mo, in agreement with the data reported here. Berns *et al.* used a reader study to identify optimum technique factors for 2, 4, 6, and 8 cm thick, 50/50 contrast-detail phantoms imaged on the GE Senographe 2000D.¹⁵ Acquisition techniques were chosen to produce constant MGD, and imaging performance was quantified by calculating the "CD score," defined as the sum of the (contrast \times diameter) products for all detected objects, averaged over six readers. Their results show that, similarly to the FOM used in this study, the CD score was a slowly changing function of kVp. For 2 and 4 cm phantom thicknesses, the CD score slowly decreased with increasing kVp, and there was little difference in score among Mo/Mo,

Mo/Rh, and Rh/Rh. By comparison, in this study for 3 cm 50/50 breasts imaged using the Senographe 2000D the FOM values for Mo/Mo and Mo/Rh were comparable but both were superior to Rh/Rh. Berns *et al.*¹⁵ found that for 6 and 8 cm thicknesses, Rh/Rh produced higher CD scores than Mo/Rh, which in turn produced higher scores than Mo/Mo, with the differences more pronounced at 8 cm than 6 cm. In this study for 7 cm 50/50 breasts the FOM values using Mo/Rh and Rh/Rh were similar and both were greater than those using Mo/Mo, while the results of Berns *et al.*¹⁵ showed a larger advantage for Rh/Rh compared to Mo/Rh for 8 cm 50/50 breasts. Thus, while the general trends in optimum target/filter selection for the Senographe 2000D are similar in the two studies, there are some differences, which is not surprising given the different FOMs used and the slightly different breast thicknesses tested.

ACKNOWLEDGMENT

The authors would like to thank Gordon Axt for his assistance with the measurements at the University of Iowa.

^{a)} Author to whom correspondence should be addressed. Present address: Department of Radiology, University of Virginia, P.O. Box 801339, Charlottesville, VA 22908. Telephone: 434-982-4422; Fax: 434-924-9435. Electronic mail: mbwilliams@virginia.edu

¹W. Huda, A. M. Sajewicz, K. M. Ogden, and D. R. Dance, "Experimental investigation of the dose and image quality characteristics of a digital mammography imaging system," *Med. Phys.* **30**, 442–448 (2003).

²M. B. Williams, M. J. More, V. Venkatakrishnan, L. Niklason, M. J. Yaffe, G. Mawdsley, A. Bloomquist, A. D. A. Maidment, D. Chakraborty, C. Kimme-Smith, and L. L. Fajardo, "Beam optimization for digital mammography," in *IWDM 2000: 5th International Workshop on Digital Mammography*, edited by M. J. Yaffe (Medical Physics, Madison, Wisconsin, 2001), pp. 108–119.

³M. B. Williams, P. Raghunathan, A. Seibert, A. Kwan, J. Lo, E. Samei, L. Fajardo, A. D. A. Maidment, and A. Bloomquist, "Beam optimization for digital mammography—II," in *Digital Mammography: Proceedings of the 8th International Workshop on Digital Mammography*, edited by S. M. Astley, M. Brandy, C. Rose, and R. Zwigelaar (Springer, Berlin,

2006), pp. 273–280.

⁴W. T. Sobol and X. Wu, "Parameterization of mammography normalized average glandular dose tables," *Med. Phys.* **24**, 547–555 (1997).

⁵L. Stanton, T. Villafana, J. Day, and D. Lightfoot, "Dosage evaluation in mammography," *Radiology* **150**, 577–584 (1984).

⁶J. M. Boone, "Glandular breast dose for monoenergetic and high-energy x-ray beams: Monte Carlo assessment," *Radiology* **213**, 23–37 (1999).

⁷J. M. Boone, G. S. Shaber, and M. Tecotzky, "Dual energy mammography: A detector analysis," *Med. Phys.* **17**, 665–675 (1990).

⁸R. L. Jennings, P. W. Quinn, R. M. Gagne, and T. R. Fewell, "Evaluation of x-ray sources for mammography," *Proc. SPIE* **1896**, 259–268 (1993).

⁹J. Y. Lo, E. Samei, J. L. Jesneck, J. T. Dobbins III, J. A. Baker, S. Singh, R. S. Saunders, and C. E. Floyd, "Radiographic technique optimization for an amorphous selenium FFDM system: Phantom measurements and initial patient results, Chapel Hill, NC, University of North Carolina at Chapel Hill," Proceedings of the IWDM 2004, 18 June 2004, 2005, pp. 31–36 (unpublished).

¹⁰E. A. Krupinski, H. Roehrig, W. Dallas, and J. Fan, "Differential use of image enhancement techniques by experienced and inexperienced observers," *J. Digit. Imaging* **18**, 311–315 (2005).

¹¹E. A. Krupinski, J. Johnson, H. Roehrig, M. Engstrom, J. Fan, J. Nafziger, J. Lubin, and W. J. Dallas, "Using a human visual system model to optimize soft-copy mammography display: Influence of MTF compensation," *Acad. Radiol.* **10**, 1030–1035 (2003).

¹²E. B. Cole *et al.*, "Diagnostic accuracy of digital mammography in patients with dense breasts who underwent problem-solving mammography: Effects of image processing and lesion type," *Radiology* **226**, 153–160 (2003).

¹³P. Bernhardt, T. Mertelmeier, and M. Hoheisel, "X-ray spectrum optimization of full-field digital mammography: Simulation and phantom study," *Med. Phys.* **33**, 4337–4349 (2006).

¹⁴T. D. Geertse, R. E. van Engen, L. J. Oostveen, M. A. O. Thijssen, and N. Karssemeijer, "Spectrum optimization for a selenium digital mammography system, Chapel Hill, NC, University of North Carolina at Chapel Hill," Proceedings of the IWDM 2004, 18 June 2004, 2005, pp. 116–122 (unpublished).

¹⁵E. A. Berns, R. E. Hendrick, and G. R. Cutter, "Optimization of technique factors for a silicon diode array full-field digital mammography system and comparison to screen-film mammography with matched average glandular dose," *Med. Phys.* **30**, 334–340 (2003).

¹⁶See EPAPS Document No. E-MPHYA6-35-010806 for a complete set of plots of FOM versus kVp for all breast thicknesses and compositions tested. For more information on EPAPS, see <http://www.aip.org/pubservs/epaps.html>.